Fibers and Polymers (2023) 24:1067–1081
https://doi.org/10.1007/s12221-023-00025-x

Online ISSN 1875-0052
Print ISSN 1229-9197

REGULAR ARTICLE

Adsorption of Malachite Green onto Walnut Shells: Kinetics, Thermodynamic, and Regeneration of the Adsorbent by Chemical Process

Samiya Merrad[1,2] · Moussa Abbas[1,3] · Mohamed Trari[2]

Received: 20 May 2021 / Revised: 9 November 2021 / Accepted: 10 December 2021 / Published online: 27 February 2023

Abstract

The textile industry produces huge amounts of wastewaters containing synthetic and toxic dyes. The aim of this study was to evaluate the adsorption of Malachite green (MG) onto Activated Carbon from Walnut Shells (ACWS) realized in a batch system. The effects of contact time, initial pH, stirring speed, particle size, temperature, adsorbent dose, and initial MG concentration on the adsorption capacity were investigated graphically for determining optimum conditions. The experimental isotherm data were analyzed by the Langmuir, Freundlich, Temkin, and Elovich models. The adsorption follows well the Langmuir equation, providing a better fit of the equilibrium adsorption data. Under optimized conditions, up to 154.56 mg/g at 25 °C and 370.37 mg/g at 45 °C were removed from the solution. The adsorption mechanism of MG onto ACWS was studied using the first-pseudo-order, second-pseudo-order, Elovich and Webber–Morris diffusion models. The adsorptions' kinetic was found to follow rather a pseudo-second-order kinetic with a determination coefficient (R^2) of 0.999. The adsorption isotherms at different temperatures have been used for the determination of thermodynamic parameters, i.e., the free energy ΔG^o (0.802 to − 2.123 kJ/mol), positive enthalpy change ΔH^o(18.547 kJ/mol), entropy ($\Delta S^o = 0.064$ kJ/molK), and activation energy ($Ea = 14.813$ kJ/mol). The negative ΔG^o and positive ΔH^o values indicate that the overall MG adsorption is spontaneous and endothermic.

Keywords Adsorption · Thermodynamic · Walnut shells · Malachite green · Modeling

1 Introduction

Several industrial segments stand out in the environmental scenario as major polluters, with a strong emphasis on the textile sector due to the volume of effluents generated, characterized by the heavily colored synthetic dyes, which do not fully bind to the fiber during the dyeing process [1]. The widespread use of synthetic dyes in the dyeing and textile industries has resulted in serious problems for human health and aquatic life worldwide due to the mutagenic, carcinogenic, and toxic properties of the dyes and their potential to contaminate water resources. Colored wastewaters arise as a direct result of the dyes production. Indeed, many dyes and their break-down products are toxic for living organisms, particularly heavy metals [2–5] and dyes. Therefore, the discoloration of malachite green (MG) is an important aspect for the water pretreatment before the discharge in the aquatic environment. The presence of dyes in the effluents affects aesthetics, water transparency, and gas solubility in water bodies, reducing the capacity of water to regenerate

✉ Moussa Abbas
m.abbas@univ-boumerdes.dz

Samiya Merrad
s.merrad@univ-boumerdes.dz

Mohamed Trari
mtrari@usthb.dz

[1] Laboratory of Soft Technologies, Valorization, Physicochemistry of Biological Materials and Biodiversity (LTDVPMBB), Faculty of Sciences, University M'hamed Bougara of Boumerdes, 35000 Boumerdes, Algeria

[2] Laboratory of Storage and Valorization of Renewable Energies, Faculty of Chemistry (USTHB), BP 32-16111 Algiers, Algeria

[3] Laboratory of Applied Chemistry and Materials (LabCAM), University of M'hamed Bougara of Boumerdes, Avenue de L'indépendance, Boumerdes 35000, Algeria

due to the lower sunlight penetration and consequent alteration of photosynthesis. Dyes can also cause allergy, dermatitis, and skin irritation, and some of them have also carcinogenic and mutagenic effects. Taking into account the volume released and the combustion of effluents, wastewater from the textile industry is classified as the most polluting of all industrial sectors. Their presence, even at very low concentrations, is visible and undesirable and may dramatically affect the photosynthetic activity of the aquatic life due to reduced light flux. Malachite green, the basic dye, is used for coloring purposes, among all other dyes in its class [6]. MG is commonly used for the dying of cotton, silk, paper, leather, manufacturing of paints, and printing inks. It is a toxic chemical and largely used to treat parasites, fungal infections, and bacterial infections in fish [7]. Despite its extensive use, MG is a highly controversial compound due to its reported toxic properties, known to cause carcinogenesis, mutagenesis, and respiratory toxicity [8]; it is hazardous and must be removed before discharge into receiving systems to prevent the environmental pollution. In this respect, adsorption is regarded as an economical and effective technique for the elimination of aqueous organic and inorganic pollutants from a variety of sources [9–14]. In contrast with other conventional treatments, such as reverse osmosis, ion exchange, electro-deposition, and precipitation, the adsorption offers the advantages of cost-effectiveness, high operational flexibility, low maintenance, simple operation, and high efficiency. Moreover, it provides an attractive alternative, especially if the adsorbent is readily available. It consists of a mass transfer operation, in which the compounds in a fluid phase are transferred to a solid phase. The adsorbed components are generally concentrated on the outer surface. The greater the surface area per unit mass of the solid, the more favorable the adsorption will be, and thus, the adsorbents are generally porous solids. Therefore, many researchers have studied the feasibility of low cost and abundant substances used for the synthesis of activated carbon. This has prompted a growing research interest in the production of activated carbons from renewable and cheaper precursors which are mainly industrial and agricultural by-products, for the water treatment. However, the commercial activated carbons are relatively expensive, and their production and regeneration cost constitute limiting factors**.** Some adsorbents, such as pomegranate peels [15], activated carbon [16, 17], soil, ground shrimp skeleton, ground oyster Shell, photocatalyst TiO_2 [18, 19], apricot stone [20], medlar nucleus [21], micro-algae [22], lingo cellulosic materials [23], polymeric nano composites [24], chitosan [25], peanut shell [26], and almond shell (*Prunus dulcis*) [27], were used for the dyes removal. To this end, the present study aims to examine the adsorption capacity of activated carbon prepared from walnut shells (ACWS) for the adsorption of malachite green. ACWS has been characterized by the different methods for the determination of the physicochemical characteristics and the effect of specified process variables like the initial pH of the solution, contact time, dose of adsorbent, stirring speed, and particle size of the solution. Adsorbent, pollutant concentration, and temperature have also been elucidated. Likewise, the experimental data generated were subjected to equilibrium and linear regression kinetics modeling and validated using a statistical error model.

2 Experimental

2.1 Materials and Methods

Analytical grade reagents were used in all experiments. Basic dye, Malachite Green (MG) was purchased from Biochem (Chemopharma) Company; its chemical and physical properties are gathered in Table 1. Malachite green dye, basic green, IUPAC name 4, [4-[[4-(Dimethylamino) phenyl]-phenylmethylidene]cyclohexa-2,5-dien-1-ylidene]-dimethylazanium; 2-hydroxy-2-oxoacetate; oxalic acid, C.I. 42,000; used as an adsorbate, chemical formula, $C_{54}H_{54}N_4O_{12}$, molecular weight, 927.00 g/mol and a maximum absorption (λ_{max} = 618 nm). A stock MG solution was prepared by dissolving 1gin 1L of distilled water and a calibration graph was constructed at λ_{max} using a UV spectrophotometer. Walnut shells used in this work come from the Souk Ahras region located east of Algiers, they were washed several times with tap water to remove dust and distilled water, and the shells are dried at 110 °C for 24 h and ground until obtaining particle sizes between 0.6 and 1 mm.The

Table 1 Characteristics of the malachite green

Properties		Structural formula
Brute formula	$C_{54}H_{54}N_4O_{12}$	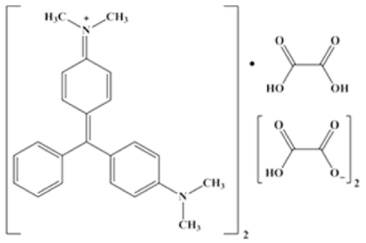
Molecular weight (g/mol)	927.00	
Composition (%)	C: 69.90, H: 5.83 O: 20.72, N: 6.04	
Wavenumber λ_{max} (nm)	618	
Name	CI 42000 Basic	
Green Malachite green	.	

dried precursor was activated with $ZnCl_2$ (*Biochem-Chem-opharma*, 98%) in a mass ratio (1/1); 5 ml of distilled water were added. The impregnate reached the interior of the particle through its natural channels producing hydrolysis reaction of the organic matter [28, 29]. The mixture was impregnated for 48 h under stirring for good homogenization. Then, it was treated in a muffle furnace (Wise Therm) under the conditions: $T = 450$ °C, $t = 30$ min and a heating gradient of 10 °C/min. ACWS was washed with HCl solution (0.1N) for 2 h under stirring, followed by distilled water until pH 6.9 and negative test with Ag^+solution. The activated carbon was dried in an oven at 110 °C for 48 h and introduced in a desiccator for 48 h to remove all traces of moisture and to sift using Afnor type sieves to finally obtain different particle sizes: (0.045–1 mm) stored in closed bottles.

The chemical analysis was performed by the X-ray fluorescence (XRF) using Horiba XRF. To observe the surface structure of the prepared ACWS before and after MG adsorption, scanning electron micrographs (SEM) were taken with different resolutions thanks to a Scanning Electron Microscope FEI model quantum 650, W.

The IR spectrums were plotted with (ATR mode) using IS50 FTIR Nicolet thermo scientific using diamond crystal; the samples were scanned in the range (4000–500 cm^{-1}) without further preparation.

2.2 Adsorption Experiments

The effects of the initial MG concentration (C_o) (30–150 mg/l), solution pH (2–10), adsorbent dose (0.1–1.2 g/l), agitation speed (150–450 rpm), and temperature (298–318 K) on the MG adsorption were studied in batch mode between 0 and 60 min. For the kinetic studies, desired quantities of ACWS were contacted with 10 ml of MG solutions in Erlenmeyer flasks and placed on a rotary shaker at 400 rpm; the aliquots were taken at regular time intervals and vigorously centrifuged (6000 rpm, 15 min) to separate the solid phases from the liquid. The remaining MG concentration was titrated with a UV–visible spectrophotometer (Perkin Elmer model 550S) at λ_{max} (=618 nm) and deduced by linear interpolation. The adsorbed quantity q_t (mg/g) and the percentage of MG elimination R_t (%) by ACWS were calculated from the following equations:

$$q_t = \frac{(C_0 - C_t) \bullet V}{m} \tag{1}$$

$$R_t = \frac{(C_0 - C_t) \bullet 100}{C_0} \tag{2}$$

C_o is the MG initial concentration and C_t is the MG concentrations (mg/l) at time (t), V the volume of solution (l), and m the mass of ACWS (g).

2.3 Error Function

For non-linear regression, the determination coefficient (R^2) is insufficient for evaluating the fit goodness. Thus, the application of error models, the Sum of Error Squares (*SSE*), and Chi-Squares (X^2) test [Eqs. (3) and (4)], respectively, are used as criteria for the quality of fitting

$$SSE = \frac{1}{N}\sum_{n=1}^{N}\left(qe_{cal} - qe_{exp}\right)^2 \tag{3}$$

$$X^2 = \sum_{1}^{N}\frac{(qe_{exp} - qe_{cal})^2}{q_{e,cal}} \tag{4}$$

where $q_{e(exp)}$ (mg/g) is the experimental uptake, $q_{e(cal)}$ the calculated uptake (mg/g), and N the number of experimental observations (the number of data points). The smaller values of *SSE* and X^2 indicate the better fitting [30, 31].

3 Results and Discussion

3.1 Characterization of the Prepared Activated Carbon (ACWS)

3.1.1 Analyses of the ACWC Composition

The X-ray fluorescence (XRF) was performed to determine the chemical composition of the adsorbent. Table 2 shows the content of chemical elements present in ACWS and the main mineralogical constituents are silica and alumina, thus-confirming the presence of Si, Al, Mg, Fe, K, P, S, O, Ca, and C. These results corroborate the XRF analysis, which confirm the presence of these elements in the oxides but in very low ratio: SiO_2, Al_2O_3, Fe_2O_3, MgO, Na_2O, CaO, K_2O, and TiO_2. The percentage of inorganic elements (0.44%) indicates that carbon is the major element of activated carbon (99.60%).

Table 2 Physicochemical characteristics of walnut shells activated by $ZnCl_2$(ACWS)

Carbonization Temperature (°C)	450
Time, (min)	30
Rate of ash (%) FX analysis	0.40
Experimental	0.50
Organic matter (%) FX analysis	99.60
Experimental	99.50
pH_{PZC}	4.05
Humidity (%)	7.7
Water content (%)	8.34

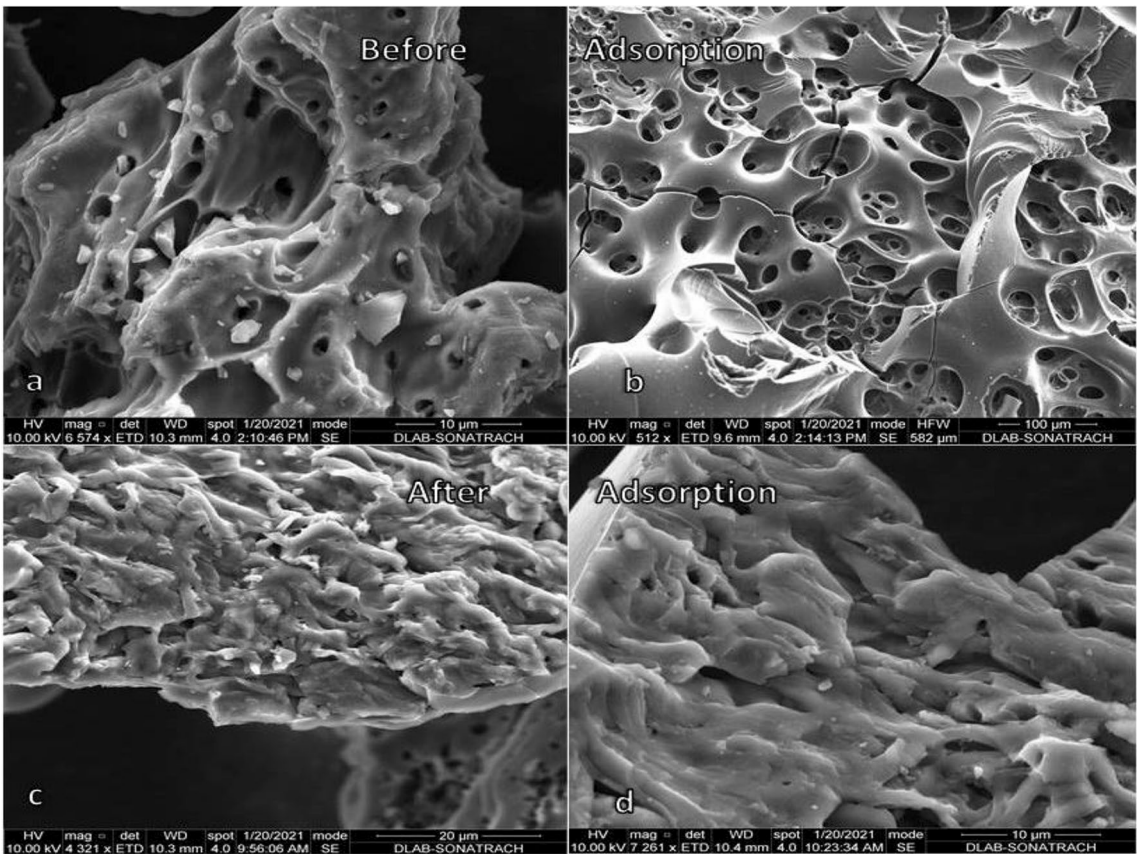

Fig. 1 Microscopic observation of the adsorbent before and after MG adsorption

3.1.2 Analyses of the ACWC Surface Morphology

The SEM micrographs of ACWS before and after adsorption are shown in Fig. 1; the prepared ACWS presents a microporous structure with different pore diameters with a rough surface and many protrusions. After adsorption, the ACWS surface became smoother where the roughness was considerably reduced with less visible pores, indicating an adsorption on both the surface and within pores. The SEM images reveal that the outer surfaces of ACWS are full of more or less homogeneous cavities of different sizes and shapes. These cavities differ from carbon to carbon in the reaction of the activating agent. These cavities are the external pores and represent the main channels to access the internal surface (micro-pores and mesopores) of the activated carbon. The higher magnification clearly shows that the adsorbent surface contains a considerable number of pores with a probability for the MG molecules to be adsorbed inside these pores.

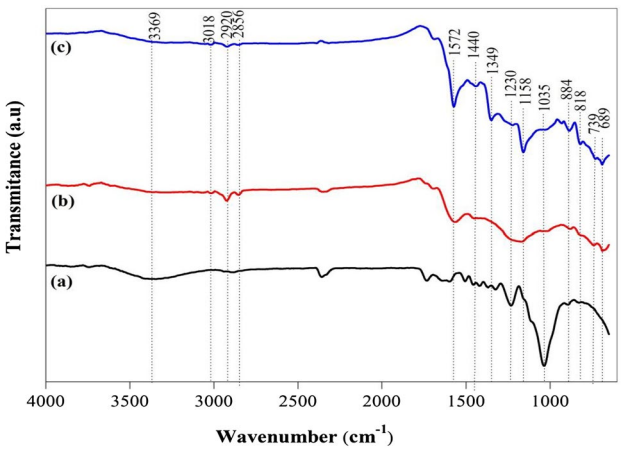

Fig. 2 IR spectrum of the Walnut Schell WS **(a)** activated ACWS **(b)** and after adsorption of the MG **(c)**

3.1.3 Analyses of the ACWC Surface Chemical

The raw material **(a)**, activated carbon **(b)**,and ACWS occupied by the MG molecules **(c)**were characterized by the infrared spectroscopy (Fig. 2). The band centered at

3369 $cm^{-1}$is attributed to both **O–H**-stretching vibration of alcohol and acidic groups **(b,c)**; it is also ascribed to **O–H** stretching of the raw material **(a)**. The bands 3018, 2920, and 2856 cm^{-1} are attributed to **C–H** symmetric and asymmetric stretching vibration modes [32].The bands 1572 and 1440 cm^{-1} are attributed to **C=C** aromatic stretching vibration with a higher intensity compared to **(b),** indicating the MG adsorption. The peak 1349 cm^{-1}, attributed to C–N stretching for the spectrum (c), also confirms the dye adsorption. The bands centered at 1230 and 1035 $cm^{-1}$are attributed to **C–O**-stretching vibrations in alcohols, phenols, or ether groups, while the peak 1158 cm^{-1} **(b,c)** is assigned to the **C–O**-stretching vibration, due to the presence of carboxyl groups [33]. The peaks 818 and 884 cm^{-1} ascribed to **C–H** deformation bands of aromatic cycles, while the alkyl group deformation corresponds to 689 cm^{-1} 739 cm^{-1}, with a high intensity in the case of MG adsorption onto ACWS.

3.2 Studies of the Effect of Process Variables

3.2.1 Effect of ACWS Size

In the first step of batch adsorption on ACWS, the effect of grain sizes on the MG uptake is examined. Figure 3 shows that the change in the adsorbed amount in the range (0.045–0.6 nm) is nearly constant, while a significant decrease is observed for the particle sizes in the range (0.6–1.0 nm). As expected, the best performance occurs with small sizes (0.045–0.075 nm) which produce a large surface area, resulting in a high MG removal capacity and removal efficiency. Therefore, this range was used in all adsorption experiments.

3.2.2 Point of Zero Charge (pH_{pzc}) and Effect of pH

The pH effect on the MG adsorption onto ACWS can be explained from the zero point charge (pH_{pzc}), and the surface functions of the material have a significant influence on the adsorption performance [34]. The basic or acidic nature of the adsorbent surface governs its retention capacity vis-à-vis to the pollutant. However, the character and chemical properties of adsorbent are directly linked to the nature of the functional groups located on its surface. The surface charge of the adsorbent, resulting from the acid–base equilibrium, depends on both the pH and ionic strength of the solution with which the material is in contact. This charge can be positive or negative depending on the environmental conditions.

Therefore, an important feature of the surface is the determination of pH_{pzc} (=4.02) (Fig. 4) by drift method which defines the pH for which the surface charge, linked to the exchange of protons, cancels out; pH_{pzc} characterizes the acidity or alkalinity of the surface. Below pH_{pzc}, the surface charge is positive (acidity) where oxygen groups are in the cationic form, which converts to negative above pH_{pzc} (alkalinity) and tends to decrease when the oxygen content increases.The pH is paramount importance in the adsorption process. It is evident that the percentage of MG removal increases with augmenting pH from 2 to 6 [33] (Fig. 5). MG is stable in the pH range (4–6) and a reduction of the color intensity increases with rising pH up to 7, the solution becomes colorless till its disappearance at pH 12 [35], the dissociation constant (pKa) is equal to 6.90, and it should be noted that the dye gets protonated in the acidic conditions and deprotonated in alkaline ones. For basic pH, the adsorption capacity of MG decreases when the pH increases, resulting from repulsive electrostatic forces between the

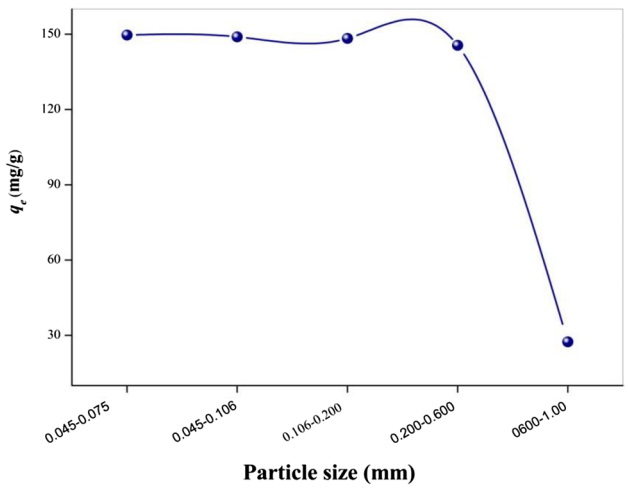

Fig. 3 Influence of the particle size on the adsorption capacity

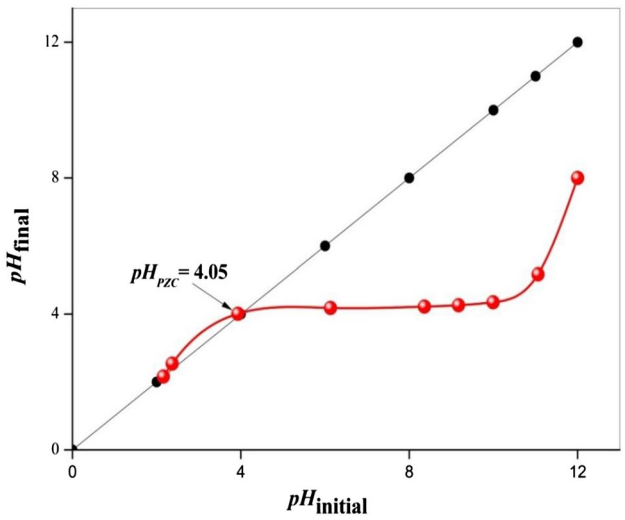

Fig. 4 Determination of the isoelectric pH (pH_{pzc})

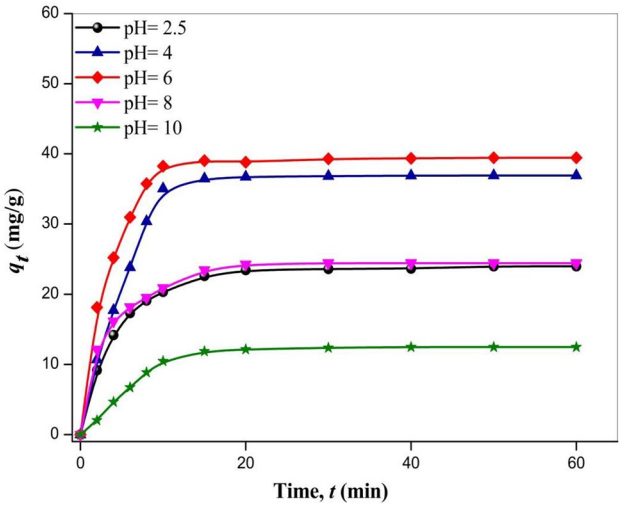

Fig. 5 Evolution of the MG adsorption onto ACWS as a function of pH

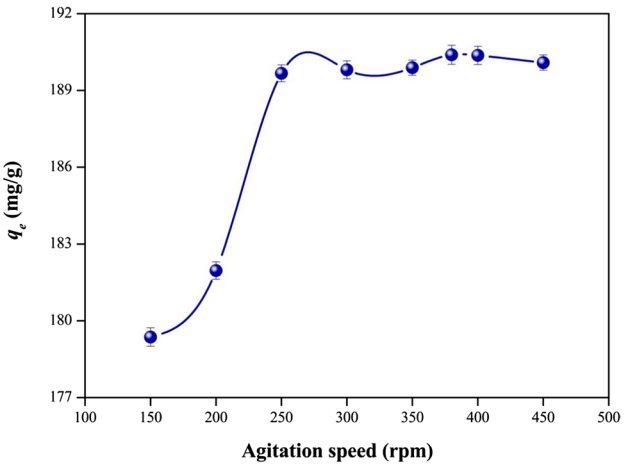

Fig. 6 Evolution of the adsorption of MG on ACWS as a function of stirring speed

adsorbent/pollutant with the same charges; similar result was obtained elsewhere [36].

3.2.3 Effect of Stirring Speed

Figure 6 illustrates the influence of the stirring speed on the MG adsorption by ACWS. The increase of the speed from 100 to 300 rpm shows a significant improvement in the MG adsorption (from 179 to 190 mg/g). For speeds between 350 and 450 rpm, the adsorption capacity remains almost constant at 192 mg/g which shows that the pores of the adsorbent are saturated, and consequently, increasing the stirring speed can cause a desorption or a vortex phenomenon or the adsorption phenomenon no longer makes sense. The

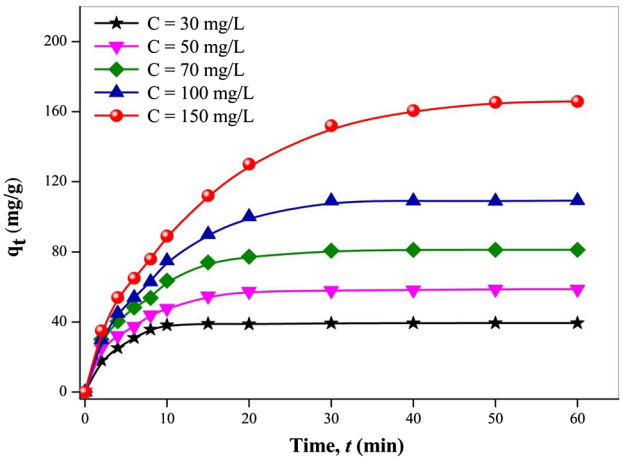

Fig. 7 Evolution of the MG adsorption at different concentrations on (ACWS) as a function of time

maximum absorption was obtained for a speed of 400 rpm. Such moderate agitation gives a good homogeneity for the suspension and prevents the vortex process. Therefore, it was retained for the rest of the parametric study and for the adsorption isotherms.

3.3 Effect of Contact Time and Initial Concentration

Figure 7 shows that the adsorption capacity of MG on ACWS increases with increasing contact time until saturation where no MG molecule can be retained; the maximal adsorption is reached after 40 min, which corresponds to the equilibrium time.

i) It is noted that when the initial MG concentration C_o ranges from 30 to 150 mg/l, the adsorbed quantity increases from 39.44 to 165.83 mg/g, resulting from the attractive electrostatic forces between the adsorbent and the pollutant, the same results were observed elsewhere [37–39]. This is due to the increase of the driving force which comes from the concentration gradient with increasing MG concentration which overcomes the resistance to the mass transfer of MG ions between the liquid and solid phases.Fast MG adsorption is due to the presence of free sites on the adsorbent surface, which reflects the linear increase of the adsorption capacity with time.

ii) Reduction of the adsorption rate, reflected by a small increase in the adsorption capacity attributed to the decrease in the MG concentration Co and the number of available unoccupied sites of ACWS.

iii) Stability of the adsorption capacity is observed, due to the total occupation of adsorption sites: the establishment of the level therefore reflects this stage.

These results clearly indicate that if the MG concentration in solution is high, there are more molecules which

diffuse toward the surface of available sites on ACWS, resulting in a significant increase in the MG retention. This phenomenon is even better perceived for the highest initial concentrations, and the adsorption mechanism can be summarized by the following steps:

1. Transfer of the pollutant from the external layer to the internal (very quick step).
2. Displacement of the bound pollutant until contact with the adsorbent (quick step).
3. Diffusion in the adsorbent under a concentration gradient (slow step).
4. Adsorption in the micro-pores (very fast step).

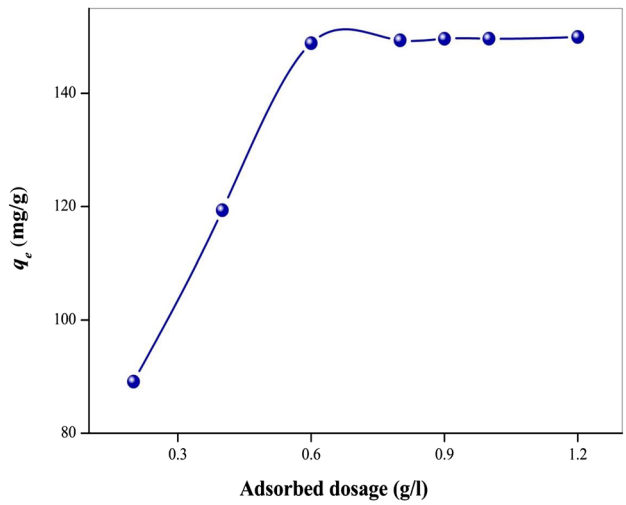

Fig. 8 Evolution of the adsorption of MG onto ACWS as a function of adsorbent dose

3.3.1 Effect of Adsorbent Dosage

Figure 8 shows the influence of the adsorbent dose on the uptake capacity of MG. Significant variations in the absorption and elimination efficiency (90–150 mg/g), indicating that the best performance is obtained in the range (0.7–1.2 g/l). The results revealed that in this range, there is no significant effect of the absorbent dose. This result was expected, because the removal efficiency augments due the increasing mass where the higher contact surface is offered to adsorption (greater availability of exchangeable sites for ions). Our results are qualitatively in good agreement with those observed elsewhere [40, 41].

3.4 Adsorption Isotherms' Modeling

The adsorption isotherm is a mathematical model that relates the equilibrium amount of the adsorbate immobilized onto the adsorbent surface (q_e) to those remaining in the solution (C_e). Several models have been documented for describing the experimental data obtained for the adsorption processes. The aim of this section is to understand the interaction dye/adsorbent through the validity of the models and to find parameters allowing comparison, interpretation, and prediction of the adsorption data of ACWS. To assess the effectiveness of adsorbent,

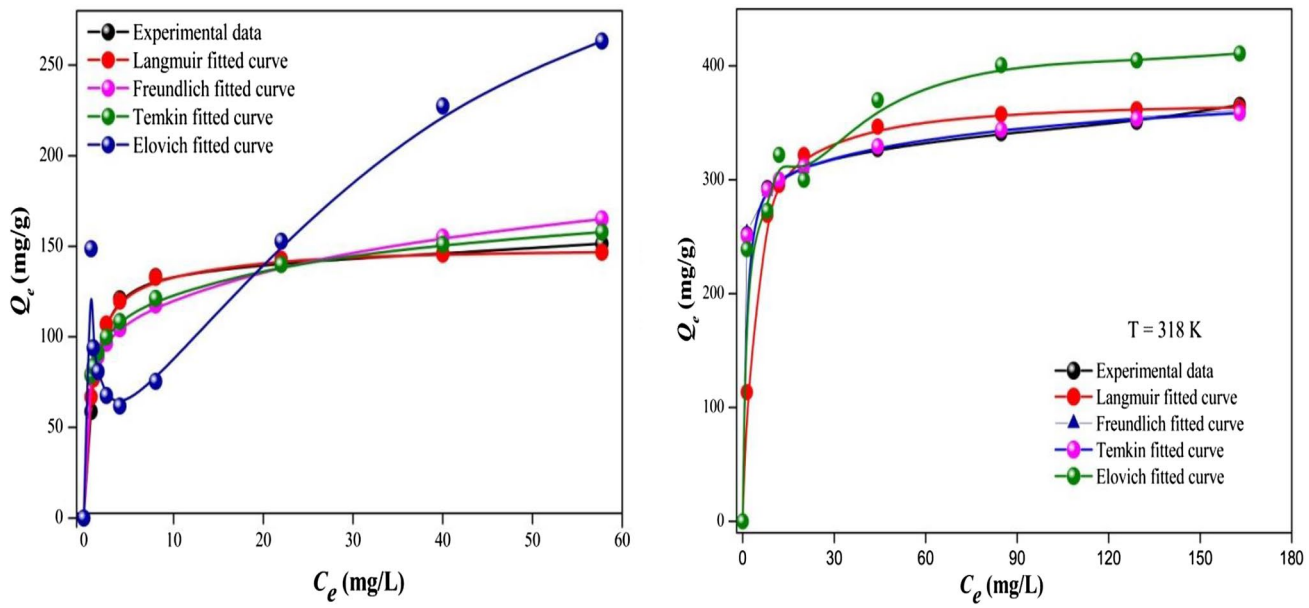

Fig. 9 Isotherms of different models at optimum conditions and different temperatures

different equations exist and are applied at optimal conditions (Fig. 9). The Langmuir model [42] postulates the occurrence of monolayer adsorption onto fixed number of localized sites on an adsorbent surface. The model further assumes that a given adsorbent surface is composed of sites homogeneously equivalent in their enthalpies but with no subsequent movement of adsorbed molecules in the surface plane, and no interactions between neighboring adsorbate molecules; the non-linear expression is given

$$qe = \frac{q_{max}.K_L.Ce}{1 + K_L.Ce}$$
$$\frac{1}{q_e} = \frac{1}{q_{max}} + \frac{1}{q_{max}.K_L.Ce} \quad (5)$$

q_{max} is the monolayer adsorption capacity (mg/g) and K_L is the constant (l/mg) related to the free adsorption energy is used to determine the dimensionless separation factor R_L, and it indicates the favorability of the adsorption process and is given by Eq. (6)

$$R_L = \frac{1}{1 + K_L \bullet C_0} \quad (6)$$

R_L indicates the type of isotherm: irreversible ($R_L = 0$), favorable ($0 < R_L < 1$), linear ($R_L = 1$), or unfavorable ($R_L > 1$). In this contribution, the R_L values are smaller than 1, thus confirming that the adsorption is favorable in both cases as well as the applicability of the Langmuir isotherm.

Freundlich's model [43] is based on the formation of unlimited multilayer's of adsorbed species, with an infinite surface coverage predicted on a heterogeneous surface. The enthalpies of the adsorbent surface sites follow a logarithmic distribution, where the higher energy sites with greater affinity for the adsorbate are occupied first, followed by the lower energy sites. The sorption process is summed across sites, and the non-linear expression of the Freundlich model is given by

$qe = K_F Ce^{1/n}$

$$lnq_e = lnK_F + \frac{1}{n} lnCe \quad (7)$$

K_F (l/g) and n are the Freundlich constants, related, respectively, to the capacity of adsorption and favorability of adsorption; the plot lnq_e versus lnC_e enables us to extract the constant K_F and n. The constant n indicates the favorability of the adsorption process. When value is between 2 and 10, favorable adsorption is expected, while an "n value" less than unity indicates poor sorption characteristics.

Similar to Freundlich's model, Temkin [44] postulates the heterogeneity of an adsorbent surface, whose adsorption energy distribution is linear; the non-linear form is given by

$q_e = (RT/b).\ln(A.Ce)$

$$q_e = B_T lnC_e + B_T lnA_T = \frac{Q_m.R.T}{\Delta Q} lnC_e + \frac{Q_m.R.T}{\Delta Q} lnA_T \quad (8)$$

$$B_T = \frac{Q_m.R.T}{\Delta Q}$$

where ΔQ(J/mol) is the Temkin adsorption energy change, andQ_m(mg/g) the maximum adsorption capacity. T(K) the absolute temperature and R the universal gas constant. The adsorption data are analyzed according to Eq. (8) and the linear plot q_e versus lnC_e permits to calculate the constants A_T and B_T.

The Elovich isotherm [45] is based on the principle of the kinetic, assuming that the number of adsorption sites augments exponentially with the adsorption, thus implying a multilayer adsorption described by

$\frac{q_e}{q_{max}} = K_E C_e.\exp\left(-\frac{q_e}{q_{max}}\right)$

Table 3 Parameters of the adsorption isotherms of the Malachite Green onto ACWS

Models	*Langmuir*	*Freundlich*	*Temkin*	*Elovich*
25 °C	K_L: 1.0152 l/mg q_{max}:149.25 mg/g	*1/n*: 0.0717 K_F: 1.361 10^2 mg/g	B_T: 18.493 A_T: 88.412 l/mg ΔQ: 20.009 kJ/mol	K_E: 78.188 l/mg q_{max}: 25.00 mg/g
R^2	0.999	0.849	0.904	0.846
SSE	0.125	2.151	7.125	12.251
X^2	0.234	3.123	10.24	14.123
45 °C	K_L: 0.331 l/mg q_{max}: 370.37 mg/g	*1/n*: 0.073 K_F: 2.48.10^2 mg/g	B_T: 22.387 A_T: 5.5 10^4 l/mg ΔQ: 43.771 kJ/mol	K_E: 22.77.10^4 l/mg q_{max}: 24.39.00 mg/g
R^2	0.998	0.992	0.988	0.988
SSE	1.021	3.123	12.124	16.235
X^2	2.123	4.123	14.123	18.124

***ΔQ** (kJ/mol): Temkin Adsorption Energy Change*

$$ln\frac{q_e}{C_e} = ln\left(q_m.K_E\right) - \frac{q_e}{q_{max}} \quad (9)$$

where K_E (l/mg) is the Elovich constant at equilibrium, q_{max} (mg/g) the maximum adsorption capacity, q_e (mg/g) the adsorption capacity at equilibrium, and C_e (g/l) the concentration of the adsorbate at equilibrium. Both the constants K_E and q_e are calculated from the plot of $ln(q_e/C_e)$ versus q_e. The constants of all models deduced after modeling are grouped in Table 3.

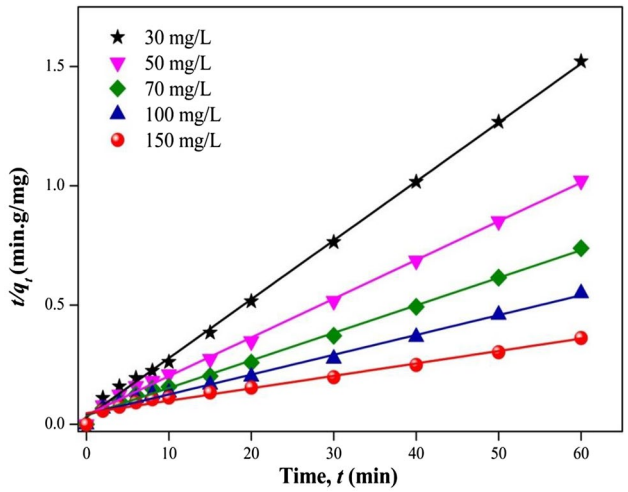

Fig. 10 Pseudo-second-order model fit for the adsorption of MG on ACWS

3.5 Adsorption Kinetic Modeling

The kinetic of MG adsorption is crucial to determine the operating conditions that are optimized for a full-scale batch process. It gives the uptake rate of adsorbate, controls the residual time of the global process, and predicts both the adsorption rate and designing of adsorption. Here also, different models were proposed to study the behavior of adsorbents and to propose the mechanisms controlling the adsorption. The experimental data of MG adsorption are examined using the pseudo-first and pseudo-second-order kinetic model given by [46, 47]

Pseudo-first-order model:

$$log\left(q_e - q_t\right) = logq_e - \frac{K_1}{2.303} \bullet t \quad (10)$$

Pseudo-second-order model

$$\frac{t}{q_t} = \frac{1}{K_2 \bullet q_e^2} + \frac{1}{q_e} \bullet t \quad (11)$$

For the pseudo-second-order, the initial adsorption rate h (mg/g.min) is expressed by

$$h = K_2 q_e^2 \quad (12)$$

where q_t (mg/g) is the adsorbed amount of MG on ACWS at the time t (min), and K_1 (min^{-1}) and K_2 (g/mg·min) are the pseudo-first-order and pseudo-second-order rate constants,

Table 4 Adsorption kinetic constants, modeled by Pseudo-First-Order and Pseudo-Second-Order, Elovich, and intraparticle equations

	Pseudo	*2nd Order*				*Pseudo*	*1st Order*		
C_o *(mg/l)*	q_{ex} *(mg/g)*	q_{cal} *(mg/g)*	R^2	$\Delta q/q$ *(%)*	K_2 *(g/mg.mn)*	q_{cal} *(mg/g)*	R^2	$\Delta q/q$ *(%)*	K_1 (mn^{-1})
30	39.443	40.502	0.998	6.38	0.0199	11.456	0.844	244.29	0.1913
50	58.723	61.576	0.996	5.6	0.0066	40.049	0.936	46.62	0.1298
70	81.274	86.580	0.994	10.89	0.0035	89.242	0.994	8.92	0.1704
100	109.170	120.337	0.988		0.0016	115.982	0.874	5.87	0.1486
150	165.834	191.939	0.972	24.39 31.25	0.0005	204.598	0.948	18.94	0.1040
		Elovich			*Diffusion*				
C_o *(mg/l)*	R^2	$1/\beta$ *(mg/g.mn)*	α *(g/mg)*		C_o *(mg/l)*	K_{in} $mg/gmn^{1/2}$	R^2	C *(mg/g)*	D cm^2/s
30	0.958	11.328	28.679		30	12.304	0.997	0.4031	$1.102\ 10^{-9}$
50	0.972	14.902			50	14.179	0.985	2.6465	
70	0.956	21.800	35.733		70	19.121	0.995	1.3674	
100	0.958	29.506			100	23.000	0.996	-0.9495	
150	0.950	37.087	37.613 35.667 41.400		150	28.818	0.995	-2.9938	

$\Delta q/q$ (%): relative error

respectively. The slope and intercept of the plots $ln(q_e\text{-}q_t)$ *vs.* time *(t)* are used to calculate the first-order rate constants K_1 and q_e, while the plot of t/q_e *vs.* t is used to determine K_2 and q_e (Fig. 10) which predict the MG uptake. For the pseudo-first-order kinetic, the experimental data deviate from linearity, as evidenced by the low values of q_e and C_o, suggesting the inapplicability of the model for the present system.

By contrast, the determination coefficient and $q_{e,cal}$ from the pseudo-second-order model agree perfectly with the experimental kinetic data; the corresponding coefficients for ACWS are summarized in Table 4. The applicability of the model suggests that the adsorption MG onto ACWS is based on a chemical reaction (chemisorption), involving an exchange of electrons between adsorbent and adsorbate where the MG ions are attached to the adsorbent surface by chemical bond.

The Elovich kinetic equation is related to the chemisorption process and is often validated for systems where the surface of the adsorbent is heterogeneous [48]; the linear form is given by

$$q_t = (\frac{1}{\beta})ln\alpha.\beta + (\frac{1}{\beta})lnt \tag{13}$$

where α (mg/gmin) is the initial adsorption rate and β (mg/g) is the relationship between the degree of surface coverage and the activation energy involved in the chemisorption.

3.5.1 Intraparticle Diffusion Equation

Generally, a process is diffusion controlled if its dependence on the rate at which the components diffuse toward one another is the limiting step. When the adsorption rate is controlled by an intraparticle diffusion mechanism which is a physical step in the adsorption process, the activation energy ($E_a = 14.813$ kJ/mol, see below) is usually very low. On the other hand, when the activation energy is high, the reaction is not controlled by intraparticle diffusion but by the number of molecules [49]. The possibility of the intraparticle diffusion [50] during the transport of adsorbate from solution to the particles surface was investigated using the intraparticle diffusion model

$$q_t = K_{in}\sqrt{t} + C \tag{14}$$

where K_{id} is the intraparticle diffusion rate (mg/g $min^{1/2}$), q_t the amount of MG adsorbed at time t, and C (mg/g) the intercept. A plot of q_t versus $t^{1/2}$ enables to determine both the constant K_{in} and C. According to Aniagor et al. [51], Fig. 11 presents a multi-linearity correlation, which indicates that two steps occur during the MG adsorption. The mechanism

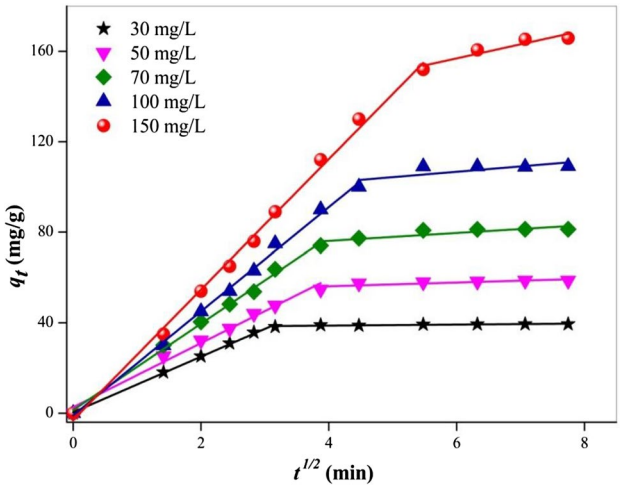

Fig. 11 Application of the intraparticle diffusion model for the adsorption of MG onto ACWS

of adsorption is complex, but the intraparticle diffusion is important in the early stages.

i. The first linear portions are due to intraparticle diffusion.
ii. The slopes of the linear parts are defined as rate parameters, characteristic of the adsorption rate in the region where the intraparticle diffusion occurs. Initially and within a short-time period, it is postulated that MG is transported to the adsorbent external surface through the film diffusion with a high rate.

After the surface saturation, the MG ions enter inside the adsorbent by intraparticle diffusion through the pores and internal surface diffusion until equilibrium is reached, evidenced by the second straight lines. The constants of the different models deduced after modeling are grouped in Table 4, which depicts an intraparticle diffusion C value, and based on literature reports, such a high value ($C>>>1$) is synonymous with the occurrence of substantive boundary layer effect within the system. Thus, the intraparticle diffusion cannot be regarded as a probable sorption mechanism in the present study.

3.5.2 Adsorption Mechanism

As previously mentioned, the intraparticle diffusion is not the only factor limiting the MG adsorption onto ACWS and other mechanisms can be involved simultaneously in the adsorption process of this system. To confirm the functional groups involved in the mechanism of MG adsorption of malachite green, we compared the FTIR spectra of the activated carbon before and after the MG adsorption (Fig. 2).

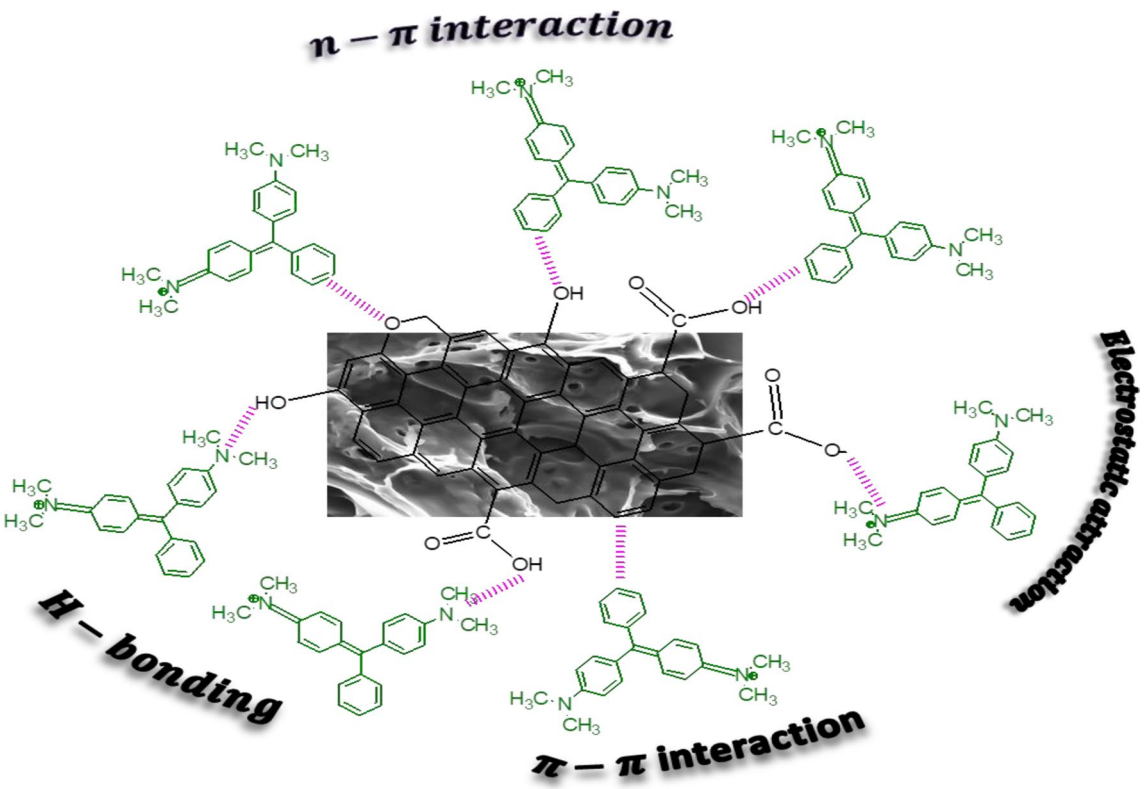

Fig. 12 Proposal for the MG adsorption mechanism by ACWS

The examination of the IR spectra obtained after adsorption confirms the attachment of MG to the activated carbon surface. In fact, we note the appearance of three absorption bands, specific to the **O–H**, **C=C**, and **C–O** groups. The position of these bands is displaced, compared to the native activated carbon, reflecting the existence of notable interactions between the MG molecules and the active sites of the carbon surface (Fig. 12). The shift of the absorption band corresponding to the hydroxyl group **O–H** confirms the formation of a hydrogen bond between MG and the activated carbon. Hydrogen bonding has occurred between H-donor atoms and acceptor groups on the surface of activated carbon. The characteristic band of aromatic group **C=C** is shifted and this reflects the presence of hydrophobic interactions of **π–π** type (Fig. 12), manifested between the π electron donor group of the aromatic ring and the acceptor group on the activated carbon surface. The characteristic **C–O** absorption band is also shifted with respect to that of the native activated carbon, thus attesting to the strong **n–π**-type interactions involved between the oxygen groups of the activated carbon, acting as an electron donor, and the aromatic ring.

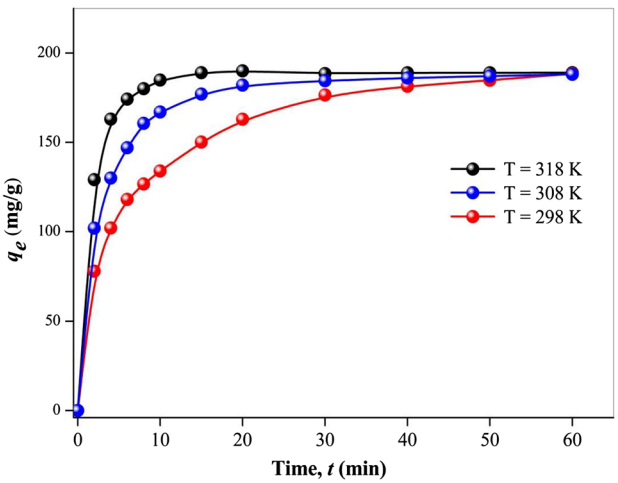

Fig. 13 Influence of temperature on the adsorption capacity of MG onto ACWS

3.6 Thermodynamic Properties of Modeling Studies

The adsorption reaction of coloring molecules on an adsorbent surface implies a variation of the free energy between the initial and final states. The adsorption of ACWS increases with increasing temperature in the range

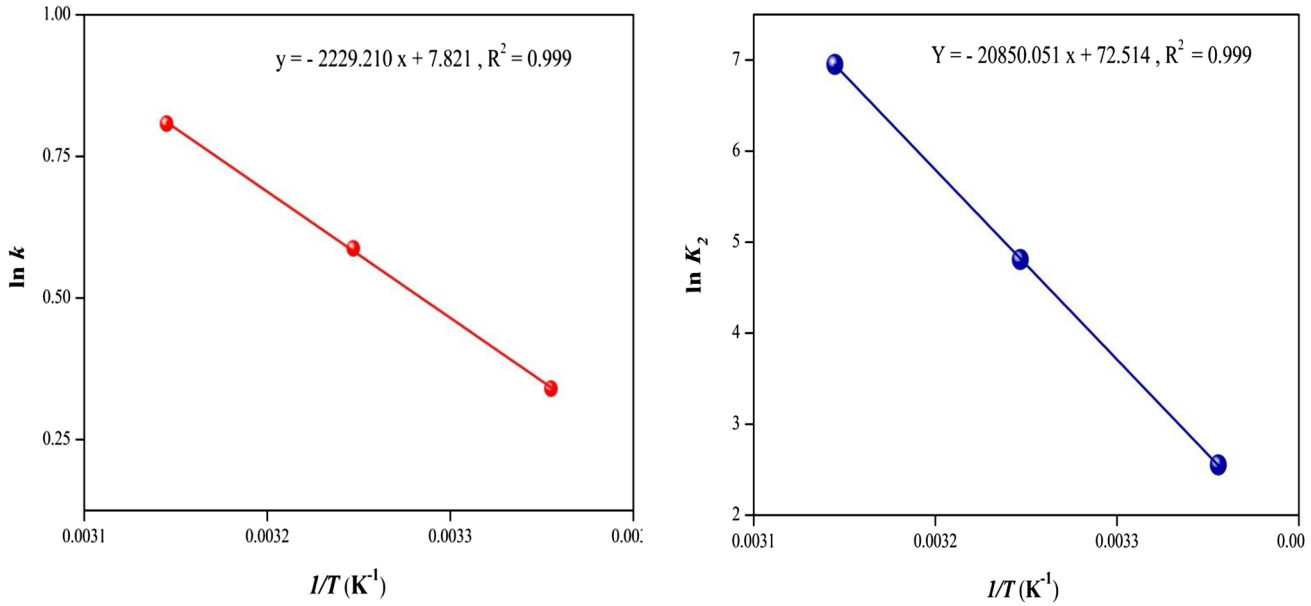

Fig. 14 Regression of the thermodynamic parameters of MG onto ACWS

(298–318 K) indicating a favorable adsorption (Fig. 13). The rates of most chemical reactions increase markedly at high temperatures with a shorter equilibrium time, generally doubling with ~ 10 °C rise in temperature. In kinetics, the temperature dependence appears in the rate constant and can be adjusted by an exponential law [52]. The constant K_2 (g/mg.min) calculated at different temperatures are gathered in Table 4

$$\ln K_2 = \ln A - \frac{Ea}{RT} \tag{15}$$

A is the pre-exponential factor. To extract the values *A* and E_a, we have reported the plots of rate constants lnq_e measured at different temperatures in the graphs lnK_2 versus *1/T*. As shown in Fig. 14a for the MG adsorption, E_a was determined from the slope of linear plots (E_a = 14.813 kJ/mol). The adsorption reaction of colored molecules on an adsorbent surface involves a variation in the free energy between the initial state and the final state. The adsorption capacity of ACWS increases with increasing temperature (298–318 K); Fig. 10 shows that the adsorption is favored at high temperature, and similar results are reported in the literature for the thermal effect [53]**.** Temperature has two important effects, known to increase the energy of mobility and the rate of diffusion of MG ions through the boundary layer and into the internal pores of the adsorbent particle, due to the decrease in the viscosity of the solution [54]**.**

The free energy change *(ΔG°)*, enthalpy *(ΔH°)*, and entropy *(ΔS°)* are calculated from the following equations:

$$\Delta G^\circ = \Delta H^\circ - T\Delta S^\circ \tag{16}$$

$$\Delta G^\circ = -RTlnK_0 \tag{17}$$

where K_o is the apparent equilibrium constant. ΔH° and ΔS° of the MG adsorption were calculated from adsorption data at different temperatures using the relation

$$ln\,K_0 = -\frac{\Delta H^\circ}{RT} + \frac{\Delta S^\circ}{R} \tag{18}$$

The values of lnK_o for thermodynamic calculations were obtained from constant K_o for the adsorption [55]. γ_1 and γ_2 are the activity coefficients of the adsorbed solute and the solute in the equilibrium suspension

Table 5 Thermodynamic functions E_a, ΔH^o, ΔS^o, and ΔG^o of the malachite green adsorbed on ACWS

T (K)	*1/T (K^{-1})*	*lnk_o*	*lnK_2 (g/mg.mn)*	*ΔG^0 (kJ/mol)*	*ΔH^0 (kJ/mol)*	*ΔS^0 (kJ/mol k)*	*Ea (kj/mol)*
298	0.003355	0.340	2.552	0.802	18.547	0.065	14.813
308	0.003247	0.588	4.812	-1.473			
318	0.003145	0.808	6.953	-2.123			

$$K_o = \frac{q_e}{C_e} \times \frac{\gamma_1}{\gamma_2} \tag{19}$$

$$\lim_{C_{e\to 0}} \frac{q_e}{C_e} = K_0 \tag{20}$$

The ratio of activity coefficients was assumed to be uniform in the dilute ranges of the solutions. As the dys concentration in the solution approaches zero, the activity coefficient tends to unity. The values of K_o determined from the intercept (figures not shown), by plotting $ln(q_e/C_e)$ versus C_e and extrapolating to $C_e = 0$. The ΔH^o and ΔS^o values obtained from the slope and intercept of the plots lnK_0versus $1/T$ (Fig. 14b) are listed in Table 5. The positive enthalpy ΔH^o and negative free energy $\Delta G°$ indicate that the MG adsorption onto ACWS is endothermic and spontaneous over the studied temperatures range [56]**.** The positive entropy ΔS^o shows that the randomness increases at the solid–solution interface during the adsorption, indicating that some structural exchange occurred between the adsorbent/MG ions.

3.7 Comparison of ACWS with Other Existing Adsorbents

The efficiency of ACWS obtained in the present work for the adsorption of Malachite green was compared with other adsorbents reported in the literature (Table 6). The pH, adsorbent dose, equilibrium time, and maximum adsorption capacity are used as comparative parameters. The absorption capacity of ACWS compared to other adsorbents is found to be a good adsorbent and could be used as an attractive candidate for the economical preparation of activated carbon.

3.8 Regeneration of the Adsorbent

Desorption is an inevitable process of adsorption and is an intermediate step toward regeneration. The latter is an essential tool to assess the reuse of any adsorbent for industrial applications, due to ecological concerns and sustainable development needs. For the regeneration of the adsorbent, several methods are distinguished among which we can mention regeneration: electrochemical, microbiological, thermal, and chemical, but we have opted for chemical regeneration because of its low economic cost. Regeneration and reuse of adsorbents for other cycles is economically important. The desorption MG of activated carbon was evaluated using three organic solvents methanol, ethanol, and acetic acid. The desorption experiments were carried

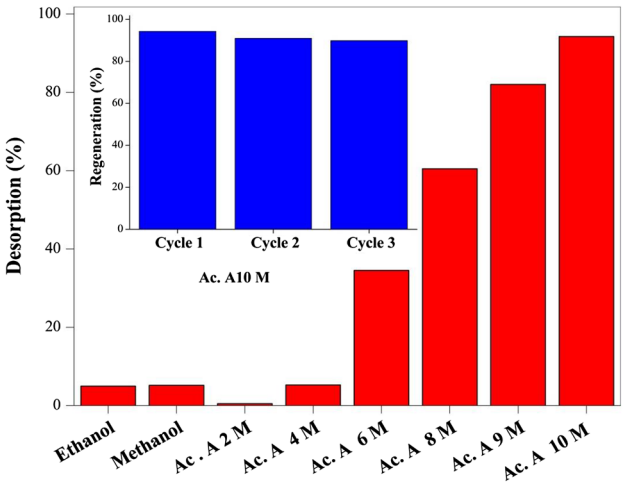

Fig. 15 Regeneration of the adsorbent

Table 6 Comparison of maximum adsorption capacities for the malachite green dye with literature data

Adsorbents	Dose (g/l)	pH	teq (h)	Q_{max} (mg/g)	Reference
Activated Carbon from Yarn Sludge (YSAC)	1.0	10.5	72	498.00	[57]
Decorated Graphene Oxide GO-CEL-Cu	1.0	7.0	1.5	202.80	[58]
SDS/CTAB@Mt	1.0	7.0	2.33	1021.45	[59]
Activated Carbon from the Epicarp of RicinusCommunis	20	7.0	0.83	27.78	[60]
Cofee Husk Treated with Sulfuric Acid(ACH)	0.2	6.8	2.0	264.82	[61]
Almond Gum	5.0	7.0	2.0	196.07	[62]
Mn-Doped CuO-NPs-AC	0.4	10.0	0.075	320.51	[63]
Fe3O4@AMCA-MIL53(Al) Nanocomposite	0.8	6.8	3.5	329.61	[40]
PinusRoxburghii Cone (PRCAC)	0.66	6.0	1.0	250.00	[64]
Apricot Stone (ASAC)	1.0	10	0.66	88.5	[6]
Shells Seeds of Ziziphus spina-christi (SZC)	1.0	6	6	48.780	[38]
Modified Shells Seeds of Ziziphus -christi SZC-AC	1.0	6	6	370.370	[38]
Elaeagnus Stone Activated Carbon (EAC)	1.0	7	1.25	432.90	[39]
H600-5N	1.0	5.1	2	192.6	[65]
Nano Chitosan from Shrimp Shells (STP)	0.3	6	3	317.73	[66]

out after adsorption of MG solution of: 150 mg/l, pH 6, adsorbent dose 0.8 g/l, particle size (0.075–0.045 mm), and temperature of 25 °C, and the activated carbon was separated from the solution by centrifugation and dehydrated at 40 °C aver night. To regenerate the activate carbon, we had kept the same conditions (adsorbent dose 0.8 g/l, particle size (0.075–0.045 mm), temperature of 25 °C, and eluting solvent of 10 ml); the carbon resulted from desorption was washed by distillated water and dehydrated overnight. Figure 15 shows that only 4.9 and 5% were desorbed using pure ethanol and methanol, respectively. By contrast, with acetic acid, the desorption was raised from 0.5% for a concentration of 1 mol/l to 94% for a concentration of 10 mol/l. Three cycles of desorption with percentages desorption of 94.91 and 89% were obtained, respectively, with acetic acid than methanol and ethanol (Fig. 15). Arabkhani and Asfaram [36] use different effluents for the MG desorption: ultrapure water, HCl, methanol, ethanol, acetone, and acetic acid, and the result revealed that the activated carbon could be recovered with a large adsorbed quantity for three cycles. Bessaha et al., [65] obtained 80% of MG desorbed using methanol, while Choudhary et al. [35] obtained a better desorption yield using KOH solution.

4 Conclusion

The experimental study on the utilization of Activated Carbon ACWS for the removal of Malachite green was investigated. The influence of different parameters, such as pH, initial dye concentration, contact time, adsorbent dose, agitation speed, and temperature, was examined. The adsorption capacity increased with augmenting the initial dye concentration, time, and pH, and the optimal pH was found to be ~ 6. The kinetics of MG removal showed an optimum contact time of 45 min via a two-stage of adsorption profile with an initial fast step followed by as low equilibrium.

The adsorption kinetic follows a pseudo-second-order model with a determination coefficients R^2 close to unity, which relies on the assumption that the chemisorptions is the rate-limiting step where the MG ions are chemically bonded to the adsorbent surface and tend to find sites which maximize their coordination number with the surface.

The equilibrium adsorption data were analyzed, indicating that the Langmuir model provides the best correlation (q_{max} = 154.56 mg/g and 370.37 mg/g at 298 K and 313 K, respectively) with a homogenous adsorption of Malachite green on monolayer ACWC sorption sites.

The adsorption isotherms at different temperatures have been used for the determination of the free energy ΔG^o (0.802 to − 2.123 kj/mol) and enthalpy ΔH^o (18.547 kj/mol), entropy (ΔS^o = 0.064 kJ/mol.K), and activation energy (E_a) 14.813 kJ/mol of adsorption. The negative ΔG^o and positive ΔH^o values indicated a spontaneous and endothermic nature of the reaction. The comparison of the adsorption capacity of the prepared adsorbent with the literature shows edits attractive properties from industrial and economic interests. The combination of high adsorption capacity and fast equilibrium suggests that this material is a noteworthy candidate for the wastewater treatment.

Acknowledgements The authors gratefully acknowledge support from the University M'hamed Bougara of Boumerdes (UMBB), Laboratory of Soft Technologies and Biodiversity, Faculty of Sciences and Laboratory of Storage and Valorization of Renewable Energies, Faculty of Chemistry (USTHB) Algeria. This research did not receive any specific grant from funding agencies in the public, commercial, or not-for-profit sectors.

Data availability No data was used for the research discribed in the article.

Declaration

Conflict of Interest The authors declare that there are no potential conflicts of interest with respect to the research, authorship, and/or publication of this article.

References

1. A.A. Inyinbor, F.A. Adekola, G.A. Olatunji, Water Resour. Ind. **15**, 14 (2016)
2. S. Yildiz, S. Sevinç, Ecol. Chem. Eng. **25**, 431 (2018)
3. S. Yıldız, M. Çekim, T. Dere, Appl. Biochem. Biotechnol. **183**, 332 (2017)
4. M. Çekim, S. Yildiz, T. Dere, J. Environ. Eng. Landscape Manage. **23**, 172 (2015)
5. S. Yildiz, Korean J. Chem. Eng. **34**, 2423 (2017)
6. M. Abbas, Adsorpt. Sci. Technol. **38**, 24 (2020)
7. A. Mittal, J. Hazard. Mater. **133**, 196 (2006)
8. I.A. Rahman, B. Saad, S. Shaidan, E.S. Sya Rizal, *Bioresour.Technol*., **96**, 1578 (2005).
9. M. Abbas, Mater. Today: Proc. **31**, 437 (2020)
10. M. Abbas, J. Water Reuse Desalin. **10**, 251 (2020)
11. M. Abbas, Z. Harrache, M. Trari, Adsorpt. Sci. Technol. **37**, 566 (2019)
12. Z. Harrache, M. Abbas, T. Aksil, M. Trari, Desalin. Water Treat. **147**, 273 (2019)
13. K. Porkodi, K.V. Kumar, J. Hazard. Mater. **143**, 311 (2007)
14. M. Abbas, T. Aksil, M. Trari, Desalin. Water Treat. **202**, 306 (2020)
15. M. Abbas, Z. Harrache, M. Trari, J. Eng. FibersFabr. **17**, 1 (2022)
16. M. Abbas, T. Aksil, M. Trari, Desalin. Water Treat. **125**, 93 (2018)
17. Z. Harrache, M. Abbas, T. Aksil, M. Trari, Microchem. J. **144**, 180 (2019)
18. M. Abbas, M. Trari, Sci. Afr. **8**, 00387 (2020)
19. M. Abbas, M. Trari, Desalin. Water Treat. **180**, 398 (2020)
20. M. Abbas, A. Cherfi, S. Kaddour, T. Aksil, M. Trari, Desalin. Water Treat. **57**, 15037 (2016)
21. M. Abbas, Mater. Today. **43**, 3359 (2021)
22. N. Daneshvar, M. Ayazloo, A.R. Khataee, M. Pourhassan, Bioresour. Technol. **98**, 1176 (2007)

23. L.W. Low, T.T. Teng, M. Rafatullah, N. Morad, B. Azahari, Sep. Sci. Technol. **48**, 1688 (2013)
24. M. Ali. Khan, R. Govindasamy, A.Ahmad, M. R.Siddiqui, S. A. Alshareef, A. A.H. Hakami, M. Rafatullah, *Polymers*,**13**, 419 (2021).
25. M. Vakili, M. Rafatullah, B. Salamatinia, A.Z. Abdullah, M.H. Ibrahim, K.B. Tan, Z. Gholami, P. Amouzgar, Carbohydr. Polym. **113**, 115 (2014)
26. S. Yildiz, Ecol. Chem. Eng S. **25**, 581 (2018)
27. S. Yildiz, Ecol. Chem. Eng S. **24**, 87 (2017)
28. A. Kumar, H.M. Jena, Appl. Surf. Sci. **356**, 753 (2015)
29. J.W. Kim, M.H. Sohn, D.S. Kim, S.M. Sohn, Y.S. Kwon, J. Hazard. Mater. **85**, 301 (2001)
30. M. Abbas, S. Kaddour, M. Trari, J. Ind. Eng. Chem. **20**, 745 (2014)
31. M. Abbas, M. Trari, Process. Safety. Environ. Prot. **98**, 424 (2015)
32. F. Guo, X. Jiang, X. Li, X. Jia, S. Liang, L. Qian, Mater. Chem. Phys. **240**, 122240 (2019)
33. A.S. Eltaweil, H.A. Mohamed, E.M.A. El-Monaem, G.M. El-Subruiti, Adv. Powder. Technol. **31**, 1253 (2020)
34. Z. Reddad, C. Gerente, Y. Andres, P. Le Cloirec, Environ. Sci. Technol. **36**, 2067 (2002)
35. M. Choudhary, R. Kumar, S. Neogi, J. Hazard. Mater. **392**, 122441 (2020)
36. P. Arabkhani, A. Asfaram, J. Hazard. Mater. **384**, 121394 (2020)
37. M. Abbas, T. Aksil, M. Trari, EC Pharmacol Toxicol. **6**, 50 (2018)
38. M.S. Bashanaini, M.H. Al-Douh, H.S. Al-Ameri, Science **7**, 42 (2019)
39. Ü. Geçgel, O. Üner, G. Göcara, Y. Bayrak, Adsorpt. Sci. Technol. **34**, 512 (2016)
40. A.A. Alqadami, M. Naushad, Z.A. Alothman, T. Ahamad, J. Environ. Manage. **223**, 29 (2018)
41. J. Yang, K. Qiu, Chem. Eng. J. **165**, 209 (2010)
42. I. Langmuir, J. Am. Chem. Soc. **40**, 1361 (1918)
43. H.M.F. Freundlich, J. Phys. Chem. **57**, 1100 (1906)
44. M.I. Temkin, Acta Physiochim. URSS. **12**, 327 (1940)
45. M. Ghaedi, F. Karimi, B. Barazesh, R. Sahraei, A. Daneshfar, J. Ind. Eng. Chem. **19**, 756 (2013)
46. S.K. Lagergren, Kung. Sven. Veten. Hand. **24**, 1 (1998)
47. Y.S. Ho, G. McKay, Process. Safety. Environ. Prot. **76**, 183 (1998)
48. R.S. Juang, M.L. Chen, Ind. Eng. Chem. Res. **36**, 813 (1997)
49. M. Doğan, M. Alkan, Chemosphere **50**, 517 (2003)
50. W.J. Weber Jr and JC. Morris, *J. Sanit. Engin. Div*., **89**, 31 (1963).
51. C.O. Aniagor, M.C. Menkiti, J. Environ. Chem. Eng. **6**, 2105 (2018)
52. K. J. Laidler, J. H. Meiser, C. Bryan, "Physical Chemistry", 4th ed., pp 365 Houghton Mifflin, (2002).
53. F. Guo, X. Jiang, X. Li, X. Jia, S. Liang, L. Qian, Mater. Chem. phys. **240**, 122240 (2020)
54. Y. Onal, C. Akmil-Basar, C. Sarıcı-Ozdemir, J. Hazard. Mater. **146**, 194 (2007)
55. Q. Li, Q.Y. Yue, Y. Su, B.Y. Gao, H.J. Sun, Chem. Eng. J. **158**, 489 (2010)
56. W. Qu, T. Yuan, G. Yin, S. Xu, Q. Zhang, H. Su, Fuel **249**, 45 (2019)
57. S.H. Tang, M.A.A. Zaini, Surf. Interfaces **22**, 100832 (2021)
58. H. Khawaja, E. Zahir, M.A. Asghar, M.A. Asghar, Int. J. Biol. Macromol. **167**, 23 (2021)
59. R. Haounati, H. Ouachtak, R. El Haouti, S. Akhouairi, F. Largo, F. Akbal, A. Benlhachemi, A. Jada, A. AitAddi, Sep. Purif. Technol. **255**, 117335 (2021)
60. T. Santhi, S. Manonmani, T. Smitha, J. Hazard. Mater. **179**, 178 (2010)
61. T.P.K. Murthy, B.S. Gowrishankar, M.N.C. Prabha, M. Kruthi, R.H. Krishna, Microchem. J. **146**, 192 (2019)
62. F. Bouaziz, M. Koubaa, F. Kallel, R.E. Ghorbel, S.E. Chaabouni, Int. J. Biol. Macromol. **105**, 56 (2017)
63. E. Sharifpour, E.Dil. Alipanahpour, A. Asfaram, M. Ghaedi, A. Goudarzi, *Appl. Organomet.Chem.*, **33**,4768 (2019).
64. G. Sharma, S. Sharma, A. Kumar, M. Naushad, B. Du, T. Ahamad, A.A Ghfar, A. A. Alqadami, F.J. Stadler, *J. Water Process Eng.*, **32**, 100931 (2019).
65. F. Bessaha, K. Marouf-Khelifa, I. Batonneau-Gener, A. Khelifa, Desalin. Water Treat. **57**, 14609 (2016)
66. S. Salamat, M. Hadavifar, H. Rezaei, J. Environ. Chem. Eng. **7**, 103328 (2019)